

On the nature of the static friction, kinetic friction and creep

B.N.J. Persson^{a,*}, O. Albohr^b, F. Mancosu^c, V. Peverì^c, V.N. Samoilov^{a,d}, I.M. Sivebaek^{a,e}

^a IFF, FZ-Jülich, 52425 Jülich, Germany

^b Pirelli Reifenwerke, 64733 Höchts/Odenwald, Postfach 1120, Germany

^c Pirelli Tire Section, Pirelli Pneumatici S.P.A., Viale Sarca 222, 20126 Milan, Italy

^d Physics Faculty, Moscow State University, 117234 Moscow, Russia

^e MEK-Energy, Technical University of Denmark, 2800 Lyngby, Denmark

Abstract

In this paper, we discuss the nature of the static and kinetic friction, and of (thermally activated) creep. We focus on boundary lubrication at high confining pressure (~ 1 GPa), as is typical for hard solids, where one or at most two layers of confined molecules separates the sliding surfaces. We find in most of our Molecular Dynamics (MD) simulations (at low sliding velocity), that the lubricant molecules are permanently attached or pinned to one of the solid walls. We describe the (flexible) lubricant-wall bonds as springs with bending elasticity. If the springs are elastically stiff, the system exhibits a very small static friction, and a (low velocity) kinetic friction which increases with increasing sliding velocity. On the other hand, if the springs are soft enough, strong elastic instabilities occur during sliding, resulting in a large static friction force F_s , and a kinetic friction force F_k equal to the static friction force at low sliding velocities. In this case rapid slip events occur at the interface, characterized by velocities much higher and independent of the drive velocity v . In the MD simulations we observe that, for incommensurate systems (at low temperature), *only when the lubrication film undergoes a phase transformation at the onset of slip do we observe a static friction coefficient which is appreciably larger than the kinetic friction coefficient*. We give arguments for why, at very low sliding velocity (where thermally activated creep occurs), the kinetic friction force may depend linearly on $\ln(v/v_0)$, as usually observed experimentally, rather than non-linearly $[-\ln(v/v_0)]^{2/3}$ as predicted by a simple theory of activated processes. We also discuss the role of elasticity at stop and start. We show that for “simple” rubber (at low start velocity), the static friction coefficient (μ_s) is equal to the kinetic friction coefficient (μ_k).

In general, at non-zero temperature, the static friction coefficient is higher than the kinetic friction coefficient because of various thermally activated relaxation processes, e.g. chain interdiffusion or (thermally activated) formation of capillary bridges. However, there is *no single value of the static friction coefficient, since it depends upon the initial dwell time and on rate of starting*. We argue that the correct basis for the Coulomb friction law, which states that the friction force is proportional to the normal load, is *not* the approximate independence of the friction coefficient on the normal pressure (which often does not hold accurately anyhow), but rather it follows from the fact that for rough surfaces the area of real contact is proportional to the load, and the pressure distribution in the contact areas is independent of the load.

© 2003 Elsevier Science B.V. All rights reserved.

PACS: 81.40.Pq; 62.20-x

Keywords: Static friction; Kinetic friction; Creep

1. Introduction

In this paper, we consider the static and kinetic friction and creep, for boundary lubricated surfaces [1,2]. We have recently presented several computer simulations of boundary lubrication for realistic model systems characterized by different (realistic) parameters [3–5]. In this paper, we will attempt to extract a general picture based on these accurate first principles studies. We hope that as more results of com-

puter “experiments” accumulate, it will confirm the present picture. We focus below on boundary lubrication at high confining pressure (~ 1 GPa) as is typical for most practical sliding systems involving hard materials, e.g. steel. Under these conditions, at low sliding velocity, one or at most two layers of confined molecules separates the sliding surfaces.

A typical sliding friction experiment is shown in Fig. 1a where a solid block is pulled by a spring, and the spring force $F(t)$ is studied as a function of time. In such experiments it is sometimes observed that the static friction equals the kinetic friction (see Fig. 1b), while for other systems they may differ by a factor of 2 or more (see Fig. 1c). It has been found that the static friction coefficient increases with the

* Corresponding author. Tel.: +49-2461-615143;

fax: +49-2461-612850.

E-mail address: b.persson@fz-juelich.de (B.N.J. Persson).

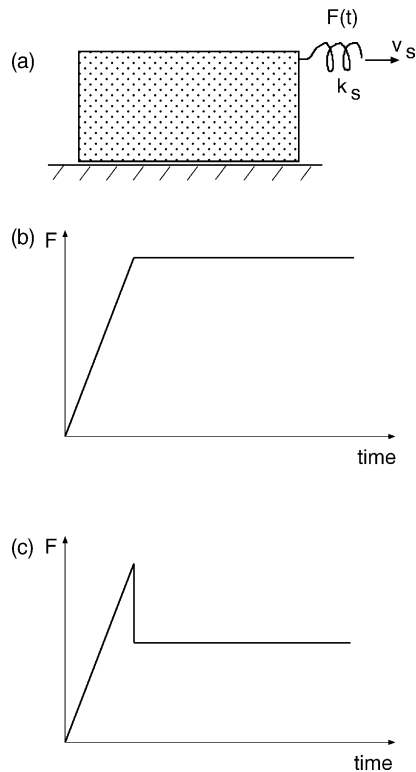


Fig. 1. (a) A block sliding on a substrate; (b) the friction force as a function of time for a case where the static friction coefficient equals the kinetic friction coefficient; (c) the friction force as a function of time for a case where the static friction coefficient is larger than the kinetic friction coefficient.

time of stationary (or static) contact, usually according to the logarithmic law [6]: $\mu_s \approx \mu_0 + a \log(1 + t/\tau)$. Similarly, the kinetic friction coefficient usually depends on the sliding velocity (for low velocities) as $\mu_k \approx \mu_1 + b \log(1 + v/v_0)$, where v_0 is a reference velocity. The time and velocity dependence of μ_s and μ_k are most likely due to thermally activated processes as will be discussed below.

Macroscopic sliding systems usually involve a large range of length scales which all must be considered when discussing the origin of the friction force. Thus, even when a block slides steadily under boundary lubrication conditions (no macroscopic stick–slip motion), rapid stick–slip motion must occur at some shorter length scale, otherwise the friction force would not be (nearly) velocity independent as observed in most cases. We illustrate this situation in Fig. 2 which shows a block sliding on a substrate. The contact between the block and the substrate occurs at randomly distributed *macrocontact* areas, with a typical diameter of a few micrometers [7]. However, when a macrocontact area is magnified one often observes that only partial contact occur. At high enough magnification the solids are in direct contact, but are usually separated by a few monolayers of (weakly adsorbed) organic molecules, either from an intentionally added lubricant or simply organic contamination from the atmosphere, or of other origin. During steady slid-

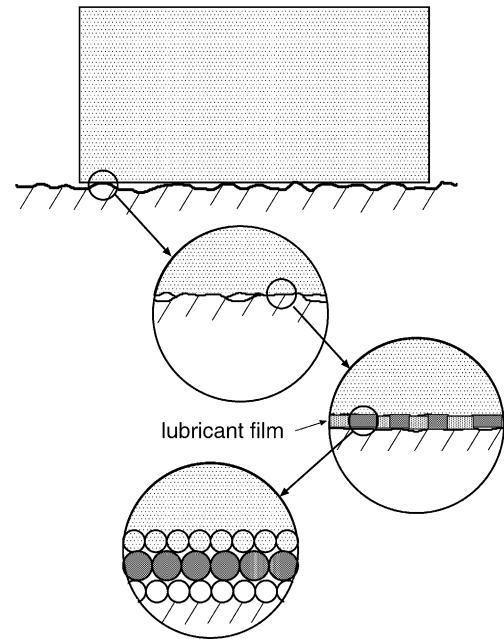


Fig. 2. A block sliding on a substrate. The contact between the block and the substrate occurs in randomly distributed *macrocontact* areas with a typical diameter of a few micrometers. However, when a macrocontact area is magnified one observes that only partial contact occur. At high enough magnification the solids are in direct contact, but are usually separated by a few monolayers of organic molecules, either from an intentionally added lubricant or simply organic contamination from the atmosphere or of other origin.

ing, stick–slip motion usually occurs at some short length scale. The short-distance stick–slip motion depends on the elasticity of the solid walls and on the interaction potentials between the contamination layer and the solid wall atoms. At low sliding velocities, a wide distribution of local stresses occurs in the lubrication film and in the surrounded solid walls at the contacting interface; the different grey-scales of the lubrication film in the inset in Fig. 2 indicate the lateral sizes of the regions where the shear stress is (approximately) constant—we denote these regions as *stress domains*, or, when the surrounding solid walls are included, *stress blocks*. During sliding at low velocities the stress blocks perform stick–slip motion, where individual stress blocks usually slip in a spatially and temporally irregular manner [8]. At finite temperatures, thermal activation will allow a stress block to depin before the shear stress has reached the value necessary for depinning at zero temperature. This gives rise to thermally activated creep and various types of relaxation processes.

In this paper, we start by discussing the motion of individual molecules (or molecular groups) at the interface, followed by a study of collective effects in lubrication films (based on Molecular Dynamics studies). We then consider the dynamics of stress blocks at zero temperature, followed by a discussion about thermally activated motion of stress blocks (creep and relaxation). Finally, we briefly discuss stick–slip and steady sliding of the macroscopic block in

Fig. 1, which depend on the spring constant k_s and pulling velocity v_s of the external spring in Fig. 1.

2. The molecular level: basic principles

In this section, we briefly review some material which form a necessary background for what follows [9–11]. Consider the sliding system shown in Fig. 3. A particle with mass m is connected via a spring, with bending force constant k , to a block or drive. The particle experiences the corrugated substrate potential $U(q)$. The equation of motion for the particle is

$$m\ddot{q} = k(x - q) - U'(q) - m\gamma_1\dot{q} - m\gamma_2(\dot{q} - \dot{x}). \quad (1)$$

The friction forces $-m\gamma_1\dot{q}$ and $-m\gamma_2(\dot{q} - \dot{x})$ originate from the coupling of the particle to the substrate and block excitations, e.g. from excitation of phonons and (for metals) electron-hole pairs. These damping processes have been studied in great detail in the context of vibrational dynamics of adsorbed molecules, but the macroscopic friction is rather insensitive to γ_1 and γ_2 , and we will not consider them any further in this paper. Let us define the total potential

$$V(q, x) = U(q) + \frac{k(x - q)^2}{2}. \quad (2)$$

We first study the equilibrium positions of the particle as a function of x . Assume for simplicity that

$$U(q) = U_0 \cos\left(\frac{2\pi q}{a}\right),$$

so that the substrate force $F(q) = -U'(q) = U_0(2\pi/a) \sin(2\pi q/a)$. At equilibrium $\ddot{q} = \dot{q} = 0$, $\dot{x} = 0$ and (1) gives

$$U_0 \left(\frac{2\pi}{a}\right) \sin\left(\frac{2\pi q}{a}\right) = k(q - x) \quad (3)$$

or

$$F(q) = k(q - x).$$

Now, it is easy to show that this equation will have exactly one solution (i.e. one stable position for the particle) when

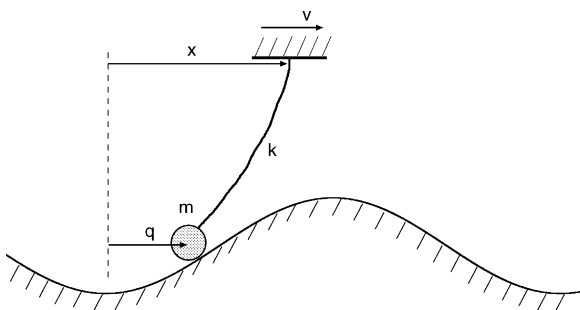


Fig. 3. A particle (mass m , coordinate q) connected to a block (or drive) (coordinate x) by a spring with the (bending) force constant k . The particle moves in a corrugated substrate potential $U(q)$.

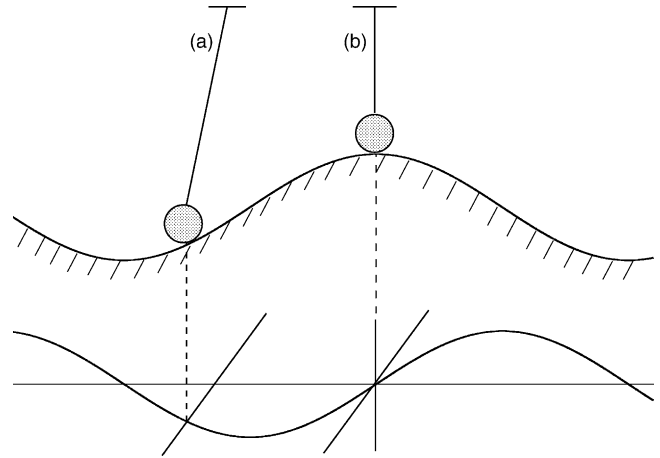


Fig. 4. (Top) Stable positions of the particle for two different positions (a) and (b) of the drive; (bottom) graphical solution of Eq. (3) for the two drive-positions shown in top. For the case $\kappa < 1$.

the largest slope (as a function of q) of the substrate force $F(q)$ is smaller than the slope k of the spring-force $k(q - x)$. In the present case the maximum of $F'(q)$ equals $U_0(2\pi/a)^2$, so that when $\kappa = U_0/\epsilon < 1$, where the elastic energy $\epsilon = ka^2/4\pi^2$, there will be only one stable position for the particle. This case is illustrated in Fig. 4. Here the top part of the figure shows the position of the particle in the potential energy surface $U(q)$ for two different positions (a) and (b) of the drive. In the bottom part of the figure we show the graphical solution to (3) for these two different cases. The tilted straight lines represent the right hand side of Eq. (3) and the crossing points with the curve $-U'(q)$ give the stable positions for the particle. It is clear that in the present case $\kappa < 1$, and only one stable position $q = f(x)$ occurs for the particle for each position x of the drive. In this case, as the drive moves slowly forward (velocity v), the particle will also move slowly with a (time-dependent) velocity $\dot{q} = f'(x)v$, proportional to v .

Let us now assume that $\kappa > 1$. In this case, Eq. (3) has more than one solution. This is illustrated in Fig. 5. In (a) we show the positions of the particle for the case when the drive is located right above a maxima of the potential $U(q)$. The graphical solution to (3) now gives three solutions denoted by A, B and C in the figure. Positions A and C are both stable while position B is unstable—any small deviation of the particle from the position B will result in the particle moving to positions A or C. It is easy to show that position B is unstable since $\partial^2 V/\partial q^2 < 0$ at this point (while the second derivative is positive at points A and C). When the drive is displaced to the right, the solutions A and B approach each other and in (b) we show a “critical” case where the drive has been displaced to the right so much that points A and B merge into a single point (denoted by A in the figure). Note that now the slope k of the spring-force line is the same as the slope of the substrate force curve at point A, i.e. $F'(q_A) = k$. Any further displacement of the drive to the right will remove the solution A. Physically, this corresponds to an instability

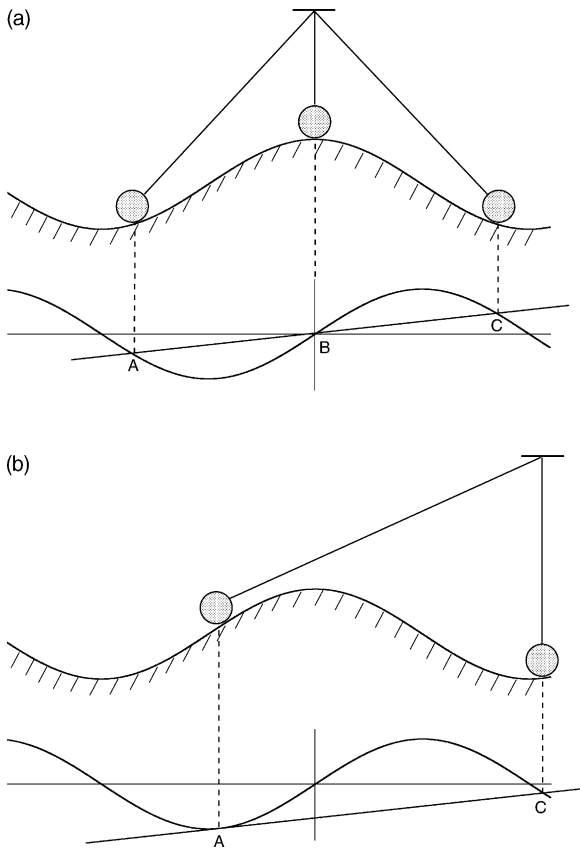


Fig. 5. (a) Particle positions (top) and graphical solution to Eq. (3) (bottom) when the drive is located above a maxima of $U(q)$; (b) the same as (a) but with the drive displaced to the right by such an amount that the system is *critical* (see text for details). We have assumed $\kappa > 1$.

transition where, in a very rapid event, the particle jumps from position A to position C. During this transition energy is “dissipated” to the block and the substrate (as described by the damping terms proportional to γ_1 and γ_2 in Eq. (1)). It is clear that during slow movement of the drive, say $x = vt$, the motion of the particle will include very rapid events where it moves from one position to another—the velocities attained by the particle in the rapid slip events are much higher than (and independent of) the velocity v of the drive.

Let us now consider the influence of temperature on the sliding process. It is clear that if the velocity v of the drive is small, when the system is close to the critical state, the particle can jump (because of a thermal fluctuation) above the small remaining barrier instead of being driven over it by the motion of the drive. To study this process, let us first note that, at the critical state (where we denote the drive position by x_c and the particle position by q_c) (point A in Fig. 5(b)), we have

$$\begin{aligned} \frac{\partial V}{\partial q}(x_c, q_c) &= 0, \\ \frac{\partial^2 V}{\partial q^2}(x_c, q_c) &= 0. \end{aligned} \tag{4}$$

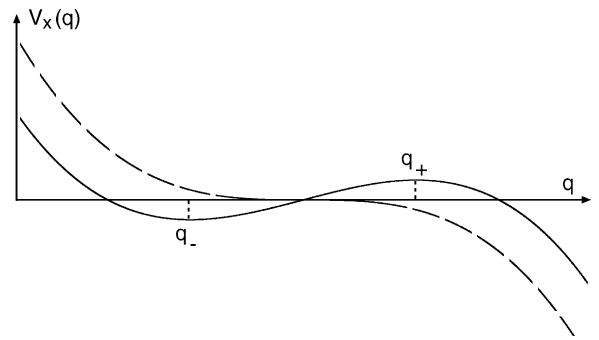


Fig. 6. The potential energy $V_x(q)$ as a function of q for the critical state $x = x_c$ (dashed curve) and for x close to x_c (solid curve).

The first condition is always satisfied at equilibrium, and just states that the total force on the particle must vanish. The second condition is characteristic of the *critical state* and follows from the fact that at point A in Fig. 5b the slope of the substrate force curve equals the slope k of the spring force line. Thus, if we expand $V(x, q)$ around (x_c, q_c) , we get:

$$\begin{aligned} V(x, q) \approx & a + b(x - x_c) + c(x - x_c)(q - q_c) \\ & + d(q - q_c)^3 + \dots \end{aligned} \tag{5}$$

Note that (4) implies that there can be no term proportional to $\sim(q - q_c)^2$ in the expansion (5). Now, let us consider $V(x, q) \equiv V_x(q)$ for a fixed x (close to x_c) as a function of q . Fig. 6 shows this function for $x = x_c$ (dashed line) and for x slightly smaller than x_c (solid line). For $x < x_c$, $V_x(q)$ exhibits a potential well separated by an *energy barrier* to a state of lower potential energy. The height of the barrier is the difference between $V(x, q)$ evaluated for $q = q_+$ and $q = q_-$, where q_{\pm} are the solutions of $\partial V/\partial q = 0$, which gives

$$q_{\pm} - q_c = \pm \left(\frac{c}{3d}\right)^{1/2} (x_c - x)^{1/2}.$$

Thus, the barrier height

$$\Delta E = V(x, q_+) - V(x, q_-) \approx \frac{8}{3} \left(\frac{c^3}{3d}\right)^{1/2} (x_c - x)^{3/2}.$$

If we assume that the drive moves with the constant velocity v and write $x = x_c + vt$ ($t < 0$), we get the time dependent barrier

$$\Delta E(t) \approx A(-vt)^{3/2},$$

where A is time independent. Using (2) one can show that

$$A = \frac{32}{3} \frac{U_0}{a^{3/2}} \frac{\pi^{3/2}}{\kappa} (\kappa^2 - 1)^{-1/4}.$$

Note that the barrier $\Delta E(t)$ vanishes for $t = 0$ (critical state), but the particle will in general jump over the barrier by thermal excitation at an earlier time $t < 0$. We can calculate

the probability that the system is in state *A* by solving the rate equation

$$\frac{dP}{dt} = -wP,$$

where the jump rate according to Kramer theory of activated processes is of the form

$$w = \nu e^{-\beta\Delta E}, \quad (6)$$

where $\beta = (1/k_B)T$ (where k_B is the Boltzmann constant and T the temperature) and where ν is a prefactor which we assume independent of time. Thus (with $t < 0$),

$$P(t) = \exp\left(-\int_{-\infty}^t dt' w(t')\right). \quad (7)$$

On the average, the particle will jump over the barrier at time $t = -\tau$ where

$$\tau = \int_{-\infty}^0 dt P'(t)t.$$

Let us introduce $P = 1 - Q$ so that $Q \rightarrow 0$ as $t \rightarrow -\infty$. Substituting this in (7) and performing a partial integration gives

$$\tau = \int_{-\infty}^0 dt Q(t)$$

or

$$\tau = \int_{-\infty}^0 dt \left[1 - \exp\left(-\int_{-\infty}^t dt' w(t')\right)\right]. \quad (8)$$

In Appendix A, we show that in the limit of very small sliding velocity $v \ll v_0$

$$v\tau \approx (\beta A)^{-2/3} \left[-\ln\left(\frac{v}{v_0}\right)\right]^{2/3}, \quad (9)$$

where

$$v_0 = \frac{2}{3}v(\beta A)^{-2/3}.$$

In the limit of overdamped motion, where the particle jumps from one well to the next nearby, and for a very weak spring k , it is very easy to estimate the velocity dependence of the sliding friction. We first note that, at zero temperature, during the time period $-\tau < t < 0$ the spring force equals $\approx kx_c$. At finite temperatures the atom has jumped to the next well so that the spring force is $\approx k(x_c - a)$. The total time it takes for the drive to move the distance a is $t_0 = a/v$. Thus, if F_0 is the (time averaged) kinetic friction force in the absence of thermal excitation (i.e. for $T = 0$ K) then at non-zero temperatures

$$F(v) = F_0 - \frac{\tau}{t_0}kx_c + \frac{\tau}{t_0}k(x_c - a) = F_0 - kv\tau$$

or using (9)

$$F(v) = F_0 - k(\beta A)^{-2/3} \left[-\ln\left(\frac{v}{v_0}\right)\right]^{2/3}. \quad (10)$$

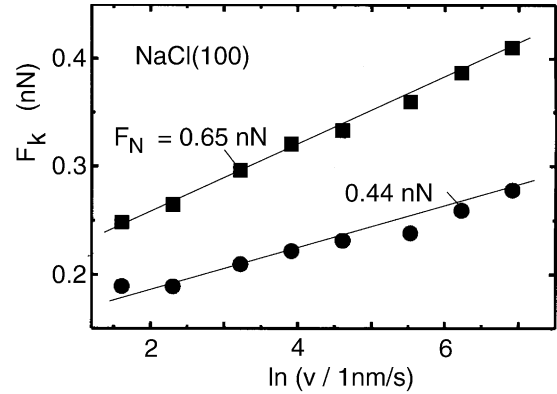


Fig. 7. Friction force F_k as a function of the sliding velocity for a silicon tip in contact with a NaCl(100) surface. Measurements at two different applied loads $F_N = 0.65$ and 0.44 nN. From [12].

This result has been derived earlier in [10,11] and may be relevant to Friction Force Microscopy (FFM) studies with a sharp tip [12]. However, a recent FFM measurements with a silicon tip sliding on a NaCl(100) surface seems to be better described by a linear dependence of the friction force on the logarithm of the sliding velocity, see Fig. 7. In Section 5, we will argue why $F(v)$ may depend linearly on $\ln(v)$ in some cases, but the argument we present is only valid if the contact area is large enough, which does not seem to be the case in the present FFM application.

Let us now consider the simple model systems shown in Fig. 8. Assume first that $T = 0$ K. Fig. 8a illustrate a case where molecular groups (e.g. chain molecules) are permanently (chemically) attached to the top solid (the “block”) with flexible bonds, which we treat as springs with bending elasticity. The solid block and the substrate are assumed to be rigid, and we assume an incommensurate system. From the discussion above it follows that if the springs are elastically stiff, so that $\kappa < 1$, then this system exhibits a vanishing static friction, and a (low velocity) kinetic friction which increases linearly with the sliding velocity v . In this case the velocities of the molecular groups at the interface, although time-dependent, will be proportional to v . On the other hand, if the springs are soft enough (compared to the

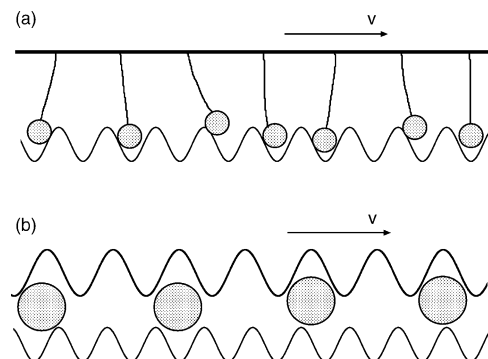


Fig. 8. Two simple sliding friction models discussed in the text.

amplitude of the corrugated substrate potential, here represented by a cosine potential) so that $\kappa > 1$, elastic instabilities will occur during sliding, resulting in a finite static friction force F_s , and a kinetic friction force F_k equal to the static friction force at low sliding velocities. In this case very rapid slip events will occur at the interface, characterized by velocities much higher and *independent* of the drive velocity v . For $T = 0$ K no motion is possible if $F < F_s$, but for $T > 0$ K the model in Fig. 8a (with $\kappa > 1$) exhibits $[-\ln(v/v_0)]^{2/3}$ -creep motion (see Eq. (10)).

Fig. 8b illustrates a case of a disordered atomic (or molecular) lubrication film between two incommensurate rigid solid walls. We assume a low concentration of lubricant molecules so that we can neglect the interaction between them. Here again two types of motion are possible: either the velocities of the lubrication molecules are of order the drive velocity v for all times, in which case the static friction coefficient vanishes, or else rapid events occur at the interface, characterized by slip velocities much higher than v (and independent of v), which result in a non-zero static friction coefficient. In the latter case one finds again that at $T = 0$ K the static friction coefficient equals the low-velocity kinetic friction coefficient.

The model in Fig. 8b is more general than that in Fig. 8a, and, in fact, the latter model can be considered as a limiting case of model (b). This is easy to show if we assume that the barrier for lateral displacement of the lubrication atoms is much larger on the surface of the block than on the substrate. In this case the lubricant atoms will be pinned in the atomic potential wells at the bottom surface of the block, and only perform displacements within these wells. If we assume that these wells are harmonic, the restoring forces can be represented by bending springs as in Fig. 8a. Depending on the magnitude of the curvature of the potential wells, $\kappa > 1$ or < 1 . If $\kappa > 1$, elastic instabilities will occur during sliding, where the atoms slip rapidly from one substrate potential well to another. That is, the lubricant layer forms a *soft compliant layer* at the interface, making elastic instabilities possible. This will (at $T = 0$ K) result in a non-zero static friction force, and a kinetic friction force which equals the static friction force. On the other hand, if $\kappa < 1$, no elastic instability will occur, and the static friction force will vanish, while the kinetic friction coefficient increases linearly with increasing drive velocity v . We point out that the pinning of the monolayer lubricant film to one of the solid walls during sliding at low velocity is observed in most computer simulations we have performed, and should therefore be very general.

3. The molecular level: numerical results

Fig. 9 shows the result of a Molecular Dynamics (MD) computer simulation, where a block is pulled on a substrate with a spring. The interface is lubricated with about 1/3-monolayer of CH₄, which forms incommensurate is-

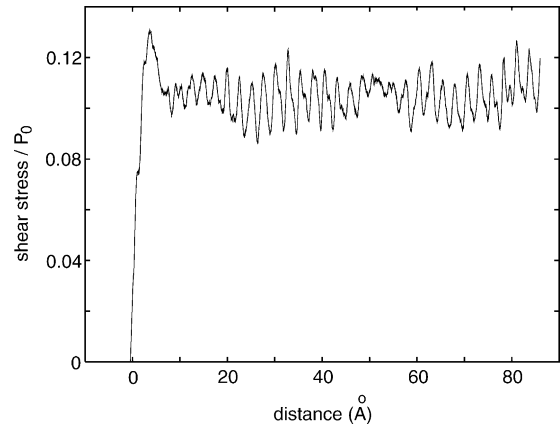


Fig. 9. Results of MD computer simulations, where a block is pulled on a substrate with a spring. The motion starts at $t = 0$ at which point the spring has its natural length. The interfacial shear stress (divided by the nominal contact pressure) is shown as a function of the distance (in Å) the spring has been pulled. In the calculations we have used: temperature $T = 10$ K, pull velocity of spring $v_s = 10$ m/s, spring constant $k_s = 30$ N/m, nominal contact pressure $P_0 = 10^8$ Pa, block mass $M = 10^6$ a.u., and the elastic modulus of the solid walls $E = 7.7 \times 10^9$ Pa.

lands between the solid walls, see Fig. 10 (note that the CH₄ molecules form a hexagonal structure). The motion starts at $t = 0$ at which point the driving spring has its natural length. The interfacial shear stress (divided by the nominal contact pressure), averaged over the contact area, is shown as a function of the distance (in Å) the spring has been pulled. In the calculations the temperature $T = 10$ K and the spring velocity $v_s = 10$ m/s. Note that steady sliding is observed and that the kinetic friction is (nearly) the same as the static friction. In the present case the solid walls are elastically relatively soft and deform (in part, because of the applied pressure and in part because of the adhesional interaction between the solid walls) in such a way as to make wall-wall contact between the CH₄ islands (see Appendix B); this is the reason why the friction coefficient is rather high in spite of the incommensurate nature of the CH₄ islands.

We note that the near equality of the static and kinetic friction force, $F_s \approx F_k$, which seems to hold (approximately)

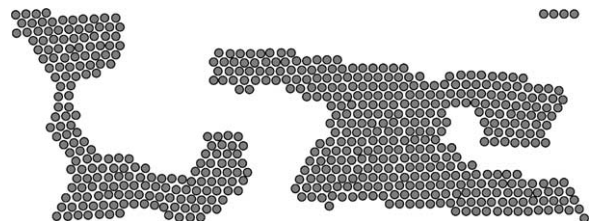


Fig. 10. Snapshot picture of a part of the contact area showing the lubrication film consisting of CH₄ molecules confined between two flat solid walls, with the block and substrate atoms removed. Note that the CH₄ molecules (locally) form a hexagonal structure which remains during sliding. However, the CH₄ islands deform and change their shapes during sliding, and different islands move with different velocities which change in a stochastic manner in time. With $E = 7.7 \times 10^9$ Pa, $T = 10$ K, $k_s = 30$ N/m, $v_s = 10$ m/s and $P = 10^8$ Pa.

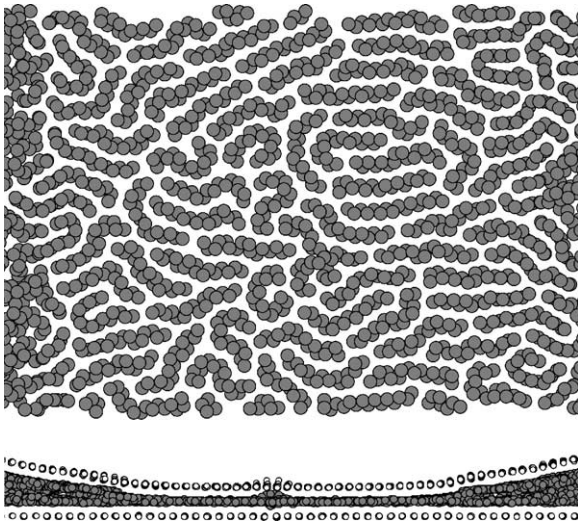


Fig. 11. Snapshot picture of the central region of the monolayer lubrication film. (Top) Top view without the block and substrate atoms; (bottom) side view of a wider region of the contact area and with the interfacial substrate and block atoms included. During slip the molecular chains $C_{16}H_{34}$ exhibit small displacements, but no net slip relative to the block, and after slip the system remains in a virtually identical state as before slip [5].

for incommensurate systems at low temperature, has been observed several times earlier, e.g. in the MD calculations of Matsukawa and Fukuyama, who studied a generalized Frenkel–Kontorova model [13]. As another illustration of the same effect, we show in Fig. 11 a case where a monolayer of $C_{16}H_{34}$ is trapped at the interface between two iron surfaces [5]. In this case the monolayer film is pinned to the block and during slip the chain molecules only perform small local displacements relative to the block. That is, during elastic loading (at low driving speed) the molecules first perform small slow displacements in their local binding potential wells, followed by rapid displacements (with velocities independent of the drive velocity) during slip. We do not observe any qualitative change in the structure of the lubrication film between the stick-state and the slip-state, and the computer simulations (see Fig. 12) show that the kinetic friction (nearly) equals the static friction.

We have found (at low temperature) that for (nearly) incommensurate systems, *only when the lubrication film undergoes a phase transformation at the onset of slip do we observe a static friction coefficient which is appreciably larger than the kinetic friction coefficient*. One such example is illustrated in Fig. 13 where a monolayer of Xe atoms is confined at the interface between two curved elastic solids [4]. In this case the monolayer goes from a domain wall super structure at stick to an incommensurate solid structure during slip, and the static friction coefficient was found to be approximately five times higher than the low-velocity kinetic friction coefficient.

Another dynamical phase transition, which sometimes is observed at the transition from stick to slip, is a transition

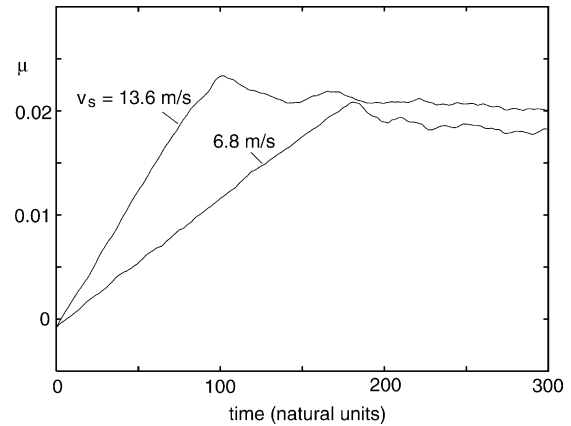


Fig. 12. The friction coefficient $\mu = F/F_N$ when a block is pulled on a substrate lubricated with a monolayer of molecular chains $C_{16}H_{34}$ (see Fig. 11). Results are shown for two different spring velocities. Note that the kinetic friction coefficient (nearly) equals the static friction coefficient.

from a solid-like state to a liquid-like state [14–16]. Here again it is observed that the static friction is much larger than the kinetic friction. At this point we note that Popov [17] has presented a simple analytical model to describe this case. The model predicts that if no phase transformation occurs

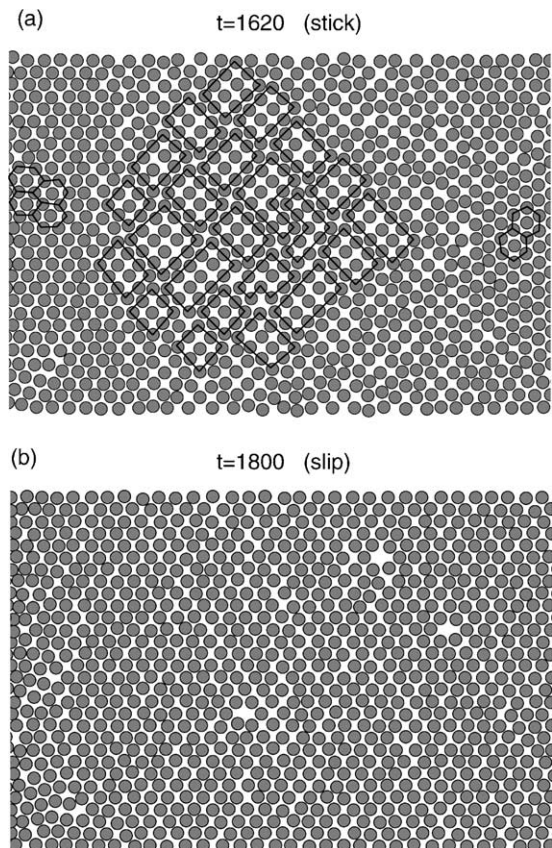


Fig. 13. Snapshot pictures of the central region of the lubrication film (a) at stick and (b) during slip. The Xe-lubricant film undergoes a dynamical phase transition at the onset of slip [4].

at the onset of slip (i.e. the sliding state is also solid-like), then μ_s is typically very close to μ_k , while a large change occur when the lubricant film shear melts at the onset of slip. However, the model assumes that the melting transformation is continuous, and it is not clear that this is the case in practice. The theory developed in [17] introduces an order parameter ϕ which is related to the shear modulus, G , of the lubricant, via $G = \phi^2$. In the solid pinned state $G > 0$ while in the fluid state $G = 0$. Thus, ϕ vanishes in the fluid state. Assuming a continuous transition one gets, in the absence of an applied shear stress, the free energy to fourth-order in ϕ :

$$F = A\phi^2 + B\phi^4,$$

where A and B are two constants. For temperatures close to the melting transition $A = \alpha(T - T_c)$, where T_c is the melting temperature. In the crystalline pinned state the lubricant film experiences a periodic potential

$$U = U_0 \cos k_0 u,$$

where $k_0 = 2\pi/a$ (where a is the lattice constant) and where u is the displacement of the lubricant film from the equilibrium position. Note that the shear modulus $G = U_0 k_0^2 d$, where d is the film thickness, so that $U_0 = \phi^2 / k_0^2 d$. When a shear stress is applied we have the total free energy

$$F = A\phi^2 + B\phi^4 + \frac{\phi^2}{k_0^2 d^2} \cos k_0 u.$$

This free energy can be considered as an effective potential from which, using standard methods, one can derive equations of motion for the variables ϕ and u . From these equations it can be shown that, if no shear melting occur at the onset of slip, in most cases the kinetic frictional shear stress is nearly equal to the static frictional shear stress. On the other hand, if shear melting occurs, then $\sigma_k \approx 0$ at low sliding velocity. This discussion focuses only on the lubrication film and does not take into account the elasticity of the solid walls. Including the elasticity will modify the picture as outlined in Section 4.

Calculations have shown that, roughly speaking, if the strength of the interatomic interaction within the lubricant layer is larger than the strength of the interaction potential with the solid walls, the solid-sliding regime is observed; otherwise the lubricant melts at the onset of sliding [18].

4. The stress-block level: zero temperature

During sliding a low speed, a very wide distribution of shear stresses is likely to occur in the macrocontact areas. The shear stress will be approximately constants over units which we denote as *stress domains* or *stress blocks* (see Fig. 14) [8]. The stress blocks in the contact area move forwards as coherent units, but (in most cases) the different blocks move in a stochastic (in time) and random (in space) manner.

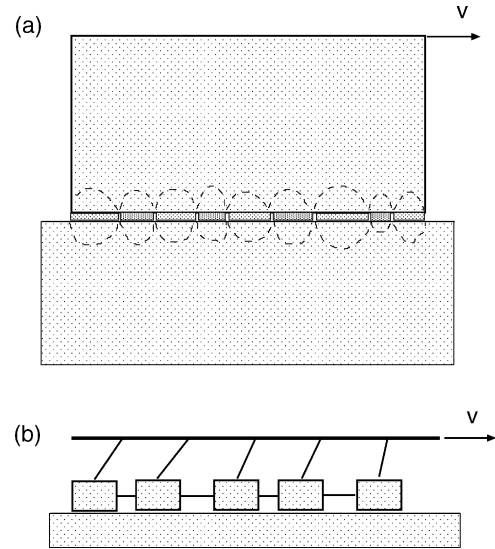


Fig. 14. (a) During sliding at very low velocity the adsorbate layer forms solid pinned domains. Associated with each domain is a stress field in the substrate and block; (b) a mechanical model used to describe the sliding properties of the interface in (a). The straight lines between the blocks, and between the blocks and the drive, denote springs with elastic properties depending on the elastic modulus of the solids.

The lateral size R of a stress block can be estimated as follows. If a shear force $F = \mu_s P_0 R^2$ (where P_0 is the contact pressure) act within the area $\sim R^2$ on the surface of a semi-infinite solid, it will give rise to a displacement of the stressed area by $u \approx F/RE$, where E is the elastic modulus of the solid. We get the size of a stress domain by putting $u \approx a$, where a is a lattice constant. Thus, we get $R \approx (E/\mu_s P_0)a$. Since typically $E/P_0 \approx 100$ and $\mu_s = 0.1$ this gives $R \approx 1000a$. Since the diameter of a macrocontact area may be a few micrometer, it is clear that it may consist of ~ 1000 stress domains.

During sliding at very low velocity the lubricant layer forms solid pinned domains, see Fig. 14a. Associated with each domain is a stress field in the substrate and block. Fig. 14b shows a mechanical model used to describe the sliding properties of the interface in (a). The straight lines between the stress blocks, and between the stress blocks and the drive, denote springs with elastic properties depending on the elastic modulus of the solids. We note, however, that most solids in the macrocontact areas may be elastically softer than in the bulk, and the springs in the figure should take this effect into account. Otherwise, one may suspect that sliding on a micron scale might occur in a coherent way, e.g. through depinning waves involving several blocks which would sweep across the junction [8,6].

Assume that at time $t = 0$ the blocks in Fig. 14 are distributed regularly (equally spaced) on the surface in such a way that the forces in the springs connected to the drive are all the same, so that the shear stress is constant at the interface. Calculations show that after a short sliding distance

the block positions becomes nearly random giving rise to a wide distribution $P(\sigma)$ of stresses at the interface [8]. Thus, we may say that the uniform stress state is *unstable*, and after a short sliding distance it converge towards a function $P^*(\sigma)$ which is independent of the sliding velocity for small sliding velocities. The kinetic frictional stress is given by [8]

$$\sigma_k = \int_{-\sigma_a}^{\sigma_a} d\sigma \sigma P^*(\sigma)$$

and at zero temperature the static frictional shear stress will be equal (or near equal) to the kinetic frictional shear stress; in a simple mean field treatment [8] they are both (at zero temperature) equal to $\sigma_a/2$. Thus, within this model *the static friction will differ from the kinetic friction only at nonzero temperatures*. In the latter case thermal excitation over the pinning barrier becomes important which result in creep motion, relaxation and memory effects in the friction dynamics (the friction at time t depend on the sliding velocity $\dot{x}(t')$ for all earlier times $t' \leq t$). In particular, at infinite long time of stationary contact (at zero applied pulling force) the stress at the interface will vanish everywhere (i.e. the stress distribution $P(\sigma) = \delta(\sigma)$), so that the static frictional shear stress is equal to σ_a , i.e. about twice the kinetic friction.

We note that computer simulations of sliding friction, such as those presented in Section 3, are usually limited to systems which are smaller than, or of order of, the stress blocks. Thus, they cannot directly be used to interpret experimental data for macroscopic systems. However, they may (in simple cases) be used to construct friction laws for the motion of the individual stress blocks, which enter as an input in computer simulations of the dynamics of the stress blocks, such as the calculations presented in [8] (which where based on the 1D model shown in Fig. 14), or more realistic 2D or 3D models [19]. For example, if it is found that the lubrication film fluidizes at the onset of slip, then it may be reasonable to assume that a stress block return to the pinned state first when the local stress reaches zero. However, in most cases *slow* interfacial processes (such as interdiffusion, see Section 7) occur, and these cannot be obtained from MD computer simulations, but may be crucial for friction dynamics at macroscopic length and time scales.

5. The stress-block level: thermally activated creep and relaxation

We have shown in the last section that without thermally activated processes, the static friction equals the kinetic friction, and no memory effects occur in the sliding dynamics. Thus, understanding the influence of temperature on motion of the the stress blocks is crucial for an understanding of friction dynamics. We have shown in [8] that many experimental observations can be very simply explained from

studies of stress block dynamics at finite temperatures. Here we would like to make some comments related to creep.

In Section 2, we briefly discussed thermally activated creep and showed that a simple model predicted a $[-\ln(v/v_0)]^{2/3}$ velocity dependence of the kinetic friction coefficient at low velocities. However, most studies of practical sliding systems find instead a linear dependence on $\ln(v/v_0)$ (see, e.g. [6]). In this section, we will discuss possible origins of this discrepancy.

The discussion of creep in Section 2 was based on the assumption that there exist a point (x_c, q_c) where the barrier vanishes and where the equation

$$\frac{\partial^2 V}{\partial q^2} = 0$$

is satisfied. Using (2) this implies that

$$\frac{\partial^2 U}{\partial q^2} = -k. \quad (11)$$

Since the spring constant k must be positive, a necessary condition for a solution to this equation is that $\partial^2 U/\partial q^2 < 0$ for some region of q , i.e. the curve $U = U(q)$ must be concave for at least some q . This is certainly the case for the cosine potential used in Section 2. However, as we will now discuss, the situation in many real applications may be more complex.

Let us first note again that for boundary lubricated surfaces, creep is likely to involve small areas or domains in the contact area which move forwards as coherent units, but in a stochastic (in time) and random (in space) manner. In Sections 1 and 4, we denoted these units as *stress domains* or *stress blocks* (see Fig. 14). In [8] (see also [19]), one of us has studied creep motion under the assumption that the stress blocks remain pinned until the local stress reaches a critical value σ_a at which point local slip start and the stress blocks moves forwards by a small amount, e.g. until the local shear stress vanishes. This picture results in a linear dependence of the kinetic friction force on $\ln(v/v_0)$, and can also describe other creep and relaxation processes observed in experiments. The origin of the $\ln(v/v_0)$ -creep law is that the barrier height depends linearly on $(x_c - x)$ for x close to x_c , rather than $\sim(x_c - x)^{3/2}$ as found for the model studied in Section 2. However, the assumption that no lateral motion occurs when the local stress $\sigma < \sigma_a$ cannot be strictly true since some displacement of the lubricant film in its pinning potential well must occur for any finite shear stress. Let us discuss this problem more in detail.

Assume first that the transition from stick to slip of the lubrication film in a stress domain is first-order as for the system considered in Fig. 13. Here the pinned state A is a domain wall superstructure while the sliding state B is an incommensurate solid structure. During sliding at low drive velocity, the system moves on an effective potential energy surface of the form shown in Fig. 15b. Fig. 15a shows (schematically) the potential energy surfaces when the

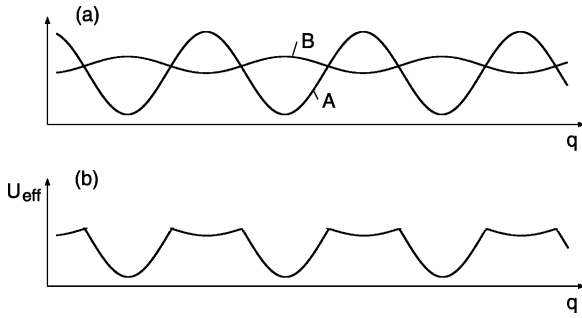


Fig. 15. (a) The potential energy surface of the stick-state (A) and the slip-state (B); (b) during sliding at low velocity the adsorbate layer fluctuates between states A and B. The system experiences the effective potential U_{eff} , where the periodicity of the potential is determined by the substrate lattice constant along the sliding direction.

system does not change its structure: note that the potential energy surface for the incommensurate state B is very flat as a result of the small change in the energy as the incommensurate system is displaced along the surface. It is clear that the effective potential U_{eff} , which is obtained by assuming that the system follows the lowest potential energy surface (and hence switch periodically between the states A and B, as indeed observed in the computer simulations), may have no point where $\partial^2 U / \partial q^2 < 0$. The same argument as above may apply if the system instead fluctuates between a pinned solid-like state at stick and a fluid-like state at slip.

At this point it is interesting to note that creep has been observed and studied for a long time in the context of flux line lattices and charge density waves [20]. These systems are usually treated as effective elastic bodies pinned by randomly distributed defects. Above a critical applied force (the depinning force) F_c , the system slides. At finite temperature slow creep motion is observed for $F < F_c$. However, the lattice does not move as a whole but small volume elements (analogous to the stress blocks introduced above) of the system move forwards in a random and incoherent manner. In this case it has been shown that even if the interaction with a pinning center (crystal defect) is assumed to be of the cosine form as in Section 2, the effective potential experienced by the moving volume elements (which contains many pinning centers) is of the “singular” form shown in Fig. 16. Thus, again, the theory described in Section 2 cannot be applied to study the creep motion of flux-line lattices or charge density wave systems but, in fact, the problem is much more complex and is not yet fully understood [21–23].

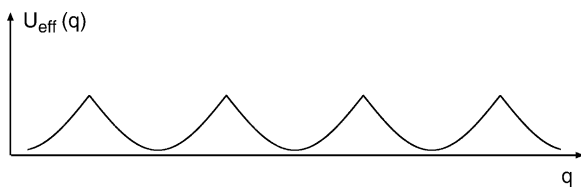


Fig. 16. The “critical” potential resulting from eliminating or “integrating out” many (short distance) degrees of freedom.

6. Macroscopic block motion: role of elasticity at stop and start

One of the most important problems in boundary lubrication is to understand the nature and origin of the transition from slip to stick and from stick to slip. We have discussed this problem in several earlier publications [24], and here we only give a few comments.

First we note that if the sliding block and the substrate are rigid then the kinetic energy of the block, $Mv^2/2$, must at stop be converted into elastic energy in the lubrication film [25], and since the latter cannot be larger than $F_s a/2$, where F_s is the static friction force and a the distance the lubricant film can be sheared before going into the sliding state (a is typically of order $\sim 1 \text{ \AA}$), we get the critical velocity $v_c \approx (F_s a/M)^{1/2}$. In particular, if only the gravitational force acts on the block so that $F_s = Mg\mu_s$ we get $v_c \approx (ga\mu_s)^{1/2} \approx 10 \text{ \mu m/s}$. This explanation for the transition from slip to stick can alternatively be considered as a block-inertia effect: to stop the motion of the block over a time period of order $\tau_1 = a/v$ requires a force of order $Mv/(a/v) = Mv^2/a$. But this force must be less than F_s in order for the stick-state to survive. This gives the same critical velocity as derived above.

However, all solids have a finite elasticity, and it is therefore not necessary to stop the motion of the whole block abruptly when going from slip to stick but instead it is enough to initially just stop the motion of the bottom surface of the block. This will result in a stopping wave propagating from the bottom surface of the block to the top surface of the block. This effect of elasticity can, in fact, be seen in the MD calculations presented in Fig. 17. After stop the shear stress at the interface oscillates in a damped manner with increasing time. This is a result of the abrupt pinning of the bottom surface of the block at the point of stick, which results in elastic deformation vibrations of the block (the frequency of the oscillations is of order c/L , where L is the height of the block and c the transverse sound velocity). Note also that immediately before “stop”, the center of mass velocity of the block is $v \approx 2 \text{ m/s}$. At “stop” the corresponding kinetic energy must be converted into deformation energy in the block (the elastic stopping wave). This “spreading out” of the stopping event in time will reduce the importance of inertia. In fact, in [24] we have studied this problem in great detail and shown that, when the elasticity of the block is taken into account, for macroscopic systems the transition from slip to stick is in most cases not determined by the inertia effect described above.

7. Macroscopic block motion: stick–slip and steady motion

We now finally arrive to the macroscopic block-level. The fundamental problem here is to understand not only the magnitude of the friction, but also how it depends on the sliding

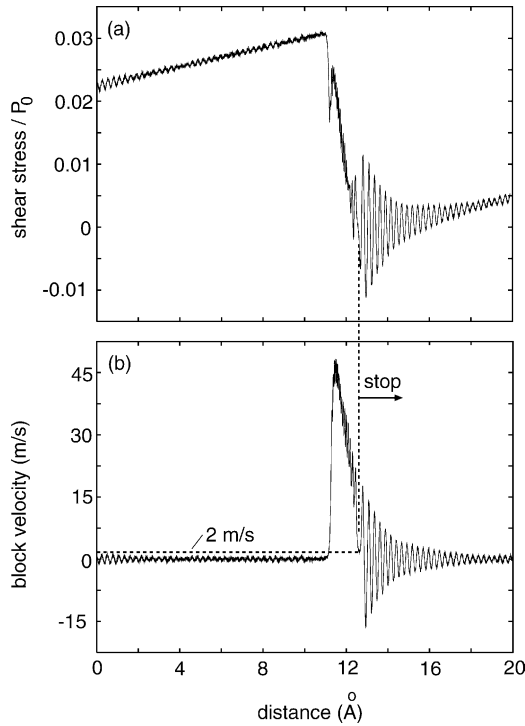


Fig. 17. Results of MD computer simulations, where a block is pulled on a substrate (lubricated by $\approx 1/3$ monolayer of CH₄) with a weak spring. Stick–slip motion is observed and the figure shows the results of one slip event. (a) The interfacial shear stress (divided by the nominal contact pressure), and (b) the block center of mass velocity, as a function of the distance (in Å) the spring has been pulled. In the calculations we have used: temperature $T = 10$ K, pull-velocity of spring $v_s = 1$ m/s, spring constant $k_s = 3$ N/m, nominal contact pressure $P_0 = 10^9$ Pa, block mass $M = 10^6$ a.u., and the elastic modulus of the solid walls $E = 7.7 \times 10^{10}$ Pa.

history (memory effects) and sliding velocity. In particular, one is interested in determining the phase boundaries in the (k_s, v_s) -plane separating stick–slip motion from steady sliding. This phase boundary, it turns out, depends sensitively on the nature of the memory effects of the friction force.

The boundary line separating steady sliding from stick–slip sliding has usually the qualitative form shown in Fig. 18. In particular, steady sliding always occur if the spring k_s is stiff enough or the velocity v_s high enough. The

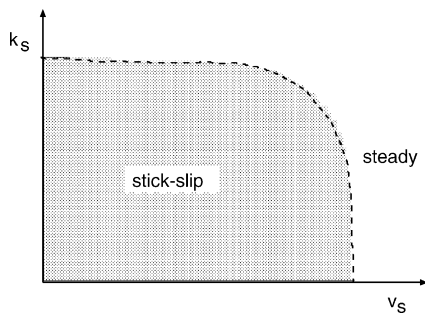


Fig. 18. Qualitative form of a typical kinetic phase diagram. In the dotted area stick–slip motion occur, while steady sliding occur in the rest of the (k_s, v_s) -plane.

position of the boundary line depends in general on whether it is approached from the steady sliding region or from the stick–slip region (hysteresis effects). We now show that all friction laws which neglect memory effects fail in describing the phase boundary in Fig. 18. To show this, assume that the kinetic friction coefficient, $\mu = \mu(v)$, only depend on the instantaneous sliding velocity $v = \dot{x}$ of the block. Let us consider the equation of motion for the block

$$M\ddot{x} = k_s[v_s t - x(t)] - F_0(\dot{x}), \quad (12)$$

where $F_0(v) = \mu(v)F_N$. Let us study when the steady sliding becomes unstable with respect to infinitesimal perturbations. We write

$$x = x_0 + v_s t + \xi,$$

so that to first-order in ξ :

$$M\ddot{\xi} = -k_s \xi - F'_0(v_s)\dot{\xi}.$$

Assuming $\xi \sim \exp(\kappa t)$ gives

$$\kappa^2 + \left[\frac{F'_0(v_s)}{M} \right] \kappa + \left(\frac{k_s}{M} \right) = 0.$$

This equation has two zeros. If the real part of the zeros are negative then the perturbation ξ of the steady motion will decay with increasing time, i.e. the steady sliding state is stable with respect to *small* perturbations. On the other hand, if a zero has a positive real part the steady motion is unstable. Thus, the line $v_s = v_s(k_s)$ in the (k_s, v_s) -plane, separating steady sliding from stick–slip motion, is determined by $\text{Re } \kappa = 0$, i.e. by $F'_0(v_s) = 0$. Note that this condition is *independent* of k_s . Thus, for all models where the friction force only depends on the instantaneous velocity of the block the $v_s = v_s(k_s)$ curve will be a *vertical line* in the (k_s, v_s) -plane. This is contrary to experimental observations, where it is found that stick–slip always can be eliminated by using a stiff enough spring k_s . However, as we will now show, it follows naturally in models where the static friction force increases monotonically with the time of stationary contact.

Let us demonstrate that if the static friction force increases with the time of stationary contact, steady sliding will occur if k_s is large enough. Assume that after the return to the pinned state the static friction force depends only on the time t of stationary contact, $F_s = F_s(t)$. We assume that $F_s(0)$ equals to the kinetic friction force at low sliding velocity just before stick (we assume overdamped motion), and that $F_s(t)$ increases monotonically with the time t of stationary contact, as shown by the solid line in Fig. 19. The dashed lines in Fig. 19 show the *spring force*, $k_s v_s t$, as a function of the time of stationary contact, for three different cases 1–3. In case 1, the spring force increases faster with time than the initial linear increase of the static friction force; hence, the motion of the block will not stop and no stick–slip motion will occur. If the spring velocity v_s is lower than the critical velocity v_c (cases 2 and 3) determined by the

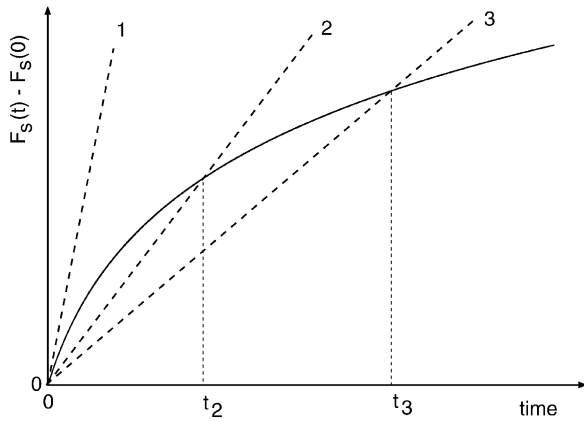


Fig. 19. (Solid line) The variation of the static friction force with the time of stationary contact; (dashed lines) the spring force for three different cases 1, 2 and 3, corresponding to the spring velocities v_1 , v_2 and v_3 , where $v_1 > v_2 > v_3$.

initial slope of the $F_s(t)$ curve [$k_s v_c = dF_s/dt(t=0)$], the spring force will be smaller than the static friction force $F_s(t)$ until t reaches the value t_2 (case 2) or t_3 (case 3), at which point slip starts. In these cases stick–slip motion will occur.

There are several different mechanisms by which the static friction force may increase with the time of stationary contact:

- Formation of capillary bridges in a humid atmosphere, see Fig. 20a. The formation of capillary bridges between non-contact regions between the block and the substrate is a thermally activated process [26,27].
- Increase in the contact area due to time dependent (thermally activated) plastic flow (perpendicular creep), see Fig. 20b. The contact area increases by the growth of existing contact areas and the formation of new contact areas [28]. Experimental data [28] and theory [29] shows that the contact area increases logarithmically with the time t of stationary contact, $A(t) = A(0) + a \ln(1+t/\tau)$.
- Chain interdiffusion for polymers, or for solids covered by grafted monolayer films, see Fig. 21. Large inter-

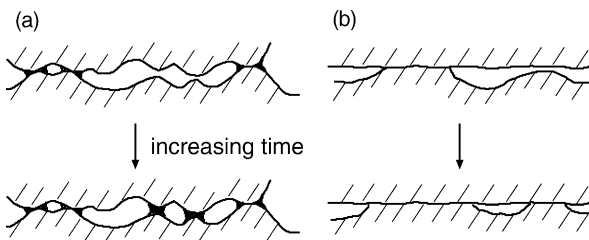


Fig. 20. Mechanisms which give rise to a strengthening of the static friction with the time of stationary contact. (a) Formation of capillary bridges. The formation of capillary bridges between non-contact regions is a thermally activated process; (b) increase in the contact area due to time dependent (thermally activated) plastic flow (perpendicular creep). The contact area increases by the growth of existing contact areas and the formation of new contact areas.

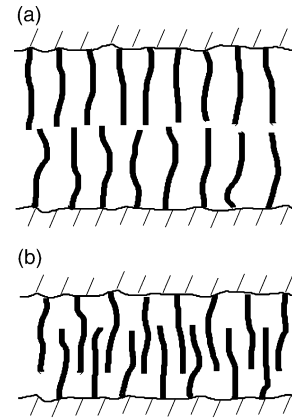


Fig. 21. Two solid surfaces with grafted monolayer films. (a) After “short” contact time; (b) after “long” contact time. Large interdiffusion is only possible if the separation between the chains is large enough and the temperature high enough.

diffusion is only possible if the separation between the chains is large enough and the temperature high enough.

- Shear stress relaxation at the interface. As discussed in Sections 4 and 5, at “stop” immediately after sliding there will be a wide distribution of local stresses at the sliding interface. With increasing time this distribution relaxes towards a $\delta(\sigma)$ -distribution for which the static friction is maximal [8].

The last process (d) operates for all sliding interfaces, while the other processes (a)–(c) may, or may not, contribute depending on the nature of contacting surfaces. Thus, for example, time dependent plastic flow occurs in most contact areas between “natural” surfaces, but for extremely smooth surfaces no plastic deformation occur and the contact is purely elastic. This is the case, e.g. in Surface Force Apparatus measurements using smooth mica surfaces. In a recent work Bureau et al. [6] have been able to study process (d) in detail by performing experiments on a rough poly(methyl methacrylate) surface in contact with a very smooth glass plate. The use of a rough/flat system enables them to take advantage of quasi-saturation associated with logarithmic growth of the contact area, by performing experimental runs of limited duration Δt on an interface of “age” $T \gg \Delta t$. Thus, during the time period Δt of the measurements, the contact area stays nearly constant. These important experiments have proved the importance of the relaxation mechanism (d).

Memory effects can be described by replacing $F_0[\dot{x}(t)]$ in (12) by a friction force $F_0[\dot{x}(t'), t' \leq t]$ which depends on the velocity of the block $\dot{x}(t')$ at all earlier times $t' \leq t$. However, in practical applications it has turned out to be much more convenient (but mathematical equivalent) to introduce one or more *state variables*, $\theta_1(t), \theta_2(t), \dots$, which obey equations of motion, and to consider the friction force as a function of $\dot{x}(t)$ and of $\theta_1(t), \theta_2(t), \dots$. By suitable choice of the state variables and of the friction law $F_0 = F_0[\dot{x}(t), \theta_1(t), \theta_2(t), \dots]$, it is possible to take into account

the processes (a)–(d) above. As an illustration, we consider a particular useful state variable, namely the “contact age” variable $\theta(t)$. This variable is assumed to satisfy the equation of motion [30]

$$\dot{\theta} = 1 - \frac{\dot{x}\theta}{D}.$$

Here D is the average displacement of the center of mass of the block (treated as a rigid object) necessary in order to break a macrocontact area, i.e. D is typically of order a few micrometers. Note that for stationary contact, $\dot{x} = 0$, we get $\theta = t$, i.e. θ equals the time of stationary contact. On the other hand, for uniform sliding $x = vt$ we get $\theta = D/v$, which is the average time a macrocontact area survives before being broken by the sliding motion. For many natural systems and for low sliding velocities, the friction force in (12) is accurately given by $F_0[\dot{x}(t), \theta(t)] = \text{constant} + A \ln \theta + B \ln \dot{x}$. This type of phenomenological approach to macroscopic friction dynamics has been very successful both for “dry” friction [30] and boundary lubrication [31,32].

A Couloumbs friction law state that the friction force is proportional to the normal load. He et al. [33] have suggested that the explanation for this fact is the (approximative) independence of the friction coefficient on the normal pressure, which often is observed at large enough pressure. However, we do not believe that this is the correct explanation in most practical applications, but rather it follows from the fact that for rough surfaces the area of real contact is proportional to the load, and the pressure distribution is independent of the load [34,35].

8. Rubber friction

Rubber friction differs in many ways from the frictional properties of most other solids. The reason for this is the very low elastic modulus of rubber and the high internal friction exhibited by rubber over a wide frequency region [36,37].

The pioneering studies of Grosch [38] have shown that rubber friction in many cases is directly related to the internal friction of the rubber. Thus, experiments with rubber surfaces sliding on silicon carbide paper and glass surfaces give friction coefficients with the same temperature dependence as that of the complex elastic modulus $E(\omega)$ of the rubber. This proves that the friction force under most normal circumstances is directly related to the internal friction of the rubber, i.e. it is mainly a *bulk property* of the rubber [38].

When rubber slides on a hard rough surface with roughness on the length scales λ , it will be exposed to fluctuating forces with frequencies $\omega \sim v/\lambda$. Since we have a wide distribution of length scales λ , we will have a corresponding wide distribution of frequency components in the Fourier decomposition of the surface stresses acting on the sliding rubber block. The time-dependent deformations of the surface region of the rubber block will result in energy

dissipation in the block which gives the major contribution to the friction force. The contribution to the friction coefficient μ from surface roughness on the length scale λ , will be maximal when $v/\lambda \approx 1/\tau$, where $1/\tau$ is the frequency where $\text{Im}E(\omega)/|E(\omega)|$ is maximal, which is located in the transition region between the rubbery region (low frequencies) and the glassy region (high frequencies). We can interpret $1/\tau$ as a characteristic rate of (thermally activated) flips of molecular segments (configurational changes), which are responsible for the visco-elastic properties of the rubber. Since the flipping is a thermally activated process it follows that τ depends exponentially (or faster) on the temperature $\tau \sim \exp(\Delta E/k_B T)$, where ΔE is the barrier involved in the transition. In reality, there is a wide distribution of barrier heights ΔE and hence of relaxation times τ , and the transition from the rubbery region to the glassy region is very wide, typically extending over three orders of magnitude in frequency. As a result of the wide distribution of substrate roughness wavelength and the large width of the loss function $\text{Im}E(\omega)/|E(\omega)|$, the kinetic friction coefficient will vary very slowly with the sliding velocity, and is very large even at extremely low sliding velocities, e.g. 10^{-10} m/s. This is illustrated in Fig. 22 which shows, for a typical case, $\mu(v)$ over a very large velocity range. The solid line is the result for a “simple” rubber with a single peak in $\mu(v)$, while the dashed curve is for a case where $\text{Im}E(\omega)/|E(\omega)|$, and hence $\mu(v)$, has two peaks as would be the case, e.g. in a mixture of two different rubbers with very different glass transition temperatures.

Let us now discuss the concept of static friction force for rubber. If there would be no interfacial pinning processes of the type described in Sections 2 and 3, then, strictly speaking, the static friction force would vanish. However, because of the wide $\mu(v)$ curve, even very small pull-velocities will result in a large (apparent) static friction coefficient.

Assume now that the kinetic friction coefficient $\mu_k(v)$ has the form shown in Fig. 22a, solid line, and that we start to pull the top surface of the rubber block with the speed v_0 indicated in Fig. 22a. In this case we would observe a static friction coefficient equal to the kinetic friction, $\mu_k(v_0)$, see solid line in Fig. 22b. If there are very low-frequency (long time) relaxation processes in the rubber (corresponding to the low-velocity peak in Fig. 22a, dashed line), they may result in a static friction force larger than the kinetic friction force under most normal sliding friction experiments [dashed line in Fig. 22b]. However, if the sliding velocity is extremely small [to the left of the low-velocity peak of $\mu(v)$] the static friction coefficient would again be equal to the kinetic friction coefficient. Thus, there is *no single value of the static friction coefficient—it depends upon the initial dwell time and rate of starting*.

It has been observed experimentally that when there is no chain interdiffusion in the contact areas, the friction force at low sliding velocity (say below 1 mm/s), usually is of the form shown by the solid line in Fig. 1b, so that the static friction equals the kinetic friction. As an example we show

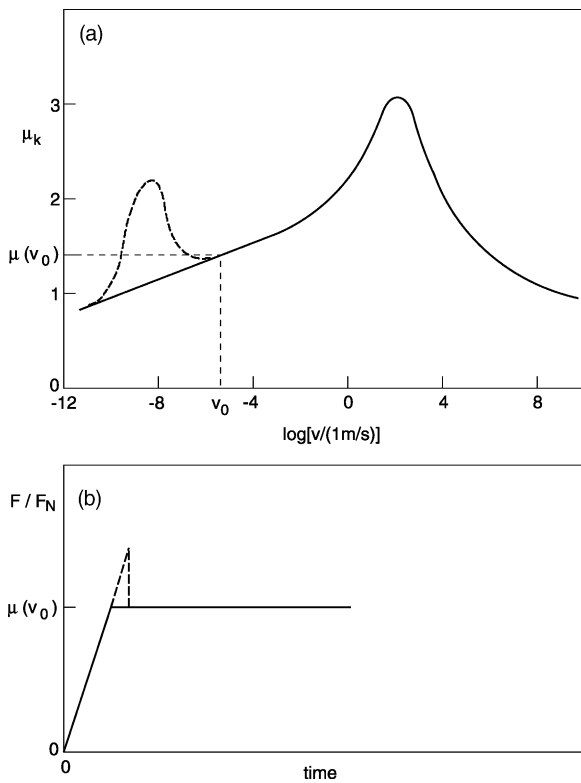


Fig. 22. (a) The steady state kinetic friction coefficient (neglecting temperature effects, e.g. by using temperature-frequency shifting in constructing the curve) for a rubber block sliding on a rough substrate. The dashed curve indicate a case where there are two maxima in $\mu(v)$ corresponding to two maxima in the mechanical loss function $\text{Im}E(\omega)/|E(\omega)|$; (b) the time dependent friction when the upper surface of the rubber block starts to move at time $t = 0$ with the speed v_0 indicated in (a).

in Fig. 23 the friction force for a rubber compounds used for tires. At $t = 0$ the upper surface of the rubber block start to move with the velocity 3.3×10^{-4} m/s, and the figure shows the force necessary to keep this constant speed. Note that $\mu_s \approx \mu_k$.

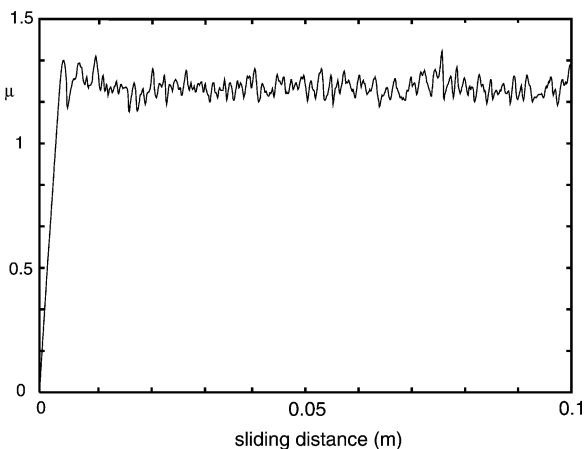


Fig. 23. Friction coefficient observed during sliding of a rubber block on a hard rough substrate at the nominal contact pressure 0.2 MPa and the sliding speed $v = 3.3 \times 10^{-4}$ m/s.

Finally, we note that in addition to the contribution to rubber friction from the internal friction of the rubber studied above, there will in general be another contribution arising from pinning effects at the interface. Thus, for a clean rubber surface (if that ever exists) in contact with a hard substrate, the rubber molecules at the interface will rearrange themselves to bind as strongly as possible to the substrate surface. Because of the lateral (atomistic) corrugation of the substrate potential this will in general give rise to an energy barrier towards sliding. However, in many practical situations this effect seems negligible, or the barriers involved are so small that they can be rapidly overcome by thermal fluctuations. If the rubber is in contact with another polymer surface, e.g. rubber in contact with rubber, chain interdiffusion may also occur at the interface which will give a contribution to the friction force (with $\mu_s > \mu_k$) [39]. Finally, since most real surfaces are contaminated with a few monolayers of physisorbed organic molecules, the contamination layer will also contribute to the friction force as discussed above. However, compared to the large contribution from the internal friction of the rubber, the latter contribution is usually negligible.

9. Summary and conclusion

In this paper, we have discussed under which conditions the static friction is larger than the kinetic friction, and related it to the nature of thermally activated creep motion. We have attempted to extract a general picture based on accurate computer simulations, and analytic studies of simple model systems. We have focused on boundary lubrication at high confining pressure (~ 1 GPa) as is typical for most practical sliding systems involving hard materials, e.g. steel. We also discussed the peculiarities of rubber friction, which is mainly a bulk property of the rubber.

The main results can be summarized as follows. We have found that in most of our MD computer simulations (at low sliding velocity), the lubricant molecules tend to be permanently attached or pinned to one of the solids, e.g. to the top solid (the “block”). If we describe the (flexible) lubricant-wall bonds as springs with bending elasticity, then if the springs are elastically stiff, the system exhibits a very small static friction, and a (low velocity) kinetic friction which increases with increasing sliding velocity. On the other hand, if the springs are soft enough, strong elastic instabilities will occur during sliding resulting in a large static friction force F_s , and a kinetic friction force F_k equal to the static friction force at low sliding velocities. In this case very rapid slip events will occur at the interface, characterized by velocities much higher and independent of the drive velocity v . In computer simulations we have found that (at low temperature) for (nearly) incommensurate systems, *only when the lubrication film undergoes a phase transformation at the onset of slip do we observe a static friction coefficient which is appreciably larger than the kinetic friction*

coefficient. We have given arguments for why, at very low sliding velocity (for which thermally activated creep occurs), the kinetic friction force may depend linearly on $\ln(v/v_0)$, as usually observed experimentally, rather than non-linearly $[-\ln(v/v_0)]^{2/3}$, as predicted by a simple theory of activated processes. We have also emphasized the important role of elasticity at stop and start. We have shown that for “simple” rubber one may expect (at low start velocity) that the static friction coefficient would be equal to the kinetic friction coefficient.

In general, at non-zero temperature, the static friction coefficient will be higher than the kinetic friction coefficient because of various thermally activated relaxation processes, e.g. chain interdiffusion or the (thermally activated) formation of capillary bridges. However, there is *no single value of the static friction coefficient, since it depends upon the initial dwell time and on the rate of starting*. We have argued that the correct basis for the Coulomb friction law, which states that the friction force is proportional to the normal load, is *not* the approximative independence of the friction coefficient on the normal pressure (which often does not hold accurately anyhow), but rather it follows from the fact that for rough surfaces the area of real contact is proportional to the load, and the pressure distribution in the contact areas is independent of the load.

Acknowledgements

B.P. thanks BMBF for a grant related to the German-Israeli Project Cooperation “Novel Tribological Strategies from the Nano- to Meso-Scales.” B.P. also acknowledges support from the European Union Smart Quasicrystals project. V.N.S. and I.M.S. acknowledge support from IFF, FZ-Jülich, hospitality and help of the staff during their research visits.

Appendix A

In this appendix we will calculate the time τ . Substituting (6) in (8) gives

$$\tau = \int_{-\infty}^0 dt \left[1 - \exp \left(-v \int_{-\infty}^t dt' e^{-\beta A(-vt')^{3/2}} \right) \right].$$

Replacing $(\beta A)^{2/3}(-vt) = y$ and $(\beta A)^{2/3}(-vt') = x$ gives

$$v\tau = (\beta A)^{-2/3} \int_0^{\infty} dy \left[1 - \exp \left(-\alpha \int_y^{\infty} dx e^{-x^{3/2}} \right) \right], \quad (\text{A.1})$$

where

$$\alpha = \frac{v}{v_0} (\beta A)^{-2/3}. \quad (\text{A.2})$$

Now, note that $\alpha \rightarrow \infty$ as $v \rightarrow 0$. As a result, for small v a very large range of y -values ($0 < y < y^*$, where y^* will be

determined below) will contribute to the integral over y in (A.1). Writing $x = y(1 + \xi)$ we get for large y :

$$\begin{aligned} \int_y^{\infty} dx e^{-x^{3/2}} &= y \int_0^{\infty} d\xi e^{-y^{3/2}(1+\xi)^{3/2}} \\ &\approx y \int_0^{\infty} d\xi e^{-y^{3/2}(1+3\xi/2)} = \frac{2}{3} y^{-1/2} e^{-y^{3/2}}. \end{aligned}$$

Now, note that

$$\frac{2}{3} \alpha y^{-1/2} e^{-y^{3/2}} = 1$$

gives

$$y^{3/2} = \ln \left(\frac{2}{3} \alpha \right) + \ln y.$$

For large α it is easy to solve this equation by iteration. To lowest order we get

$$y \approx \left[\ln \left(\frac{2}{3} \alpha \right) \right]^{2/3} \equiv y^*.$$

We can now approximate the integral (A1) with

$$v\tau \approx (\beta A)^{-2/3} \int_0^{y^*} dy = (\beta A)^{-2/3} \left[\ln \left(\frac{2}{3} \alpha \right) \right]^{2/3}$$

or

$$v\tau \approx (\beta A)^{-2/3} \left[-\ln \left(\frac{v}{v_0} \right) \right]^{2/3}, \quad (\text{A.3})$$

where

$$v_0 = \frac{2}{3} v (\beta A)^{-2/3}. \quad (\text{A.4})$$

Appendix B

In this appendix we present more results for the sliding of flat surfaces separated by $\approx 1/3$ monolayer of CH_4 . Let us first briefly return to the system displayed in Fig. 10. We will address the following questions:

1. Why is the friction coefficient so high ($\mu \approx 0.1$) when the CH_4 molecules form islands which are (nearly) incommensurate with the block and the substrate?
2. During sliding we observe that the CH_4 islands merge into larger islands. Why?

The answer to both questions is related to the fact that because of the relatively low elastic modulus of the solids, the external pressure and the wall–wall adhesion interaction will deform the solids so that complete wall–wall contact occurs between the CH_4 islands (see Fig. 24a). In the wall–wall contact areas, the wall atoms form domain wall super structures, where the area between the domain walls consist of (1×1) domains (where the block atoms are in registry with the substrate atoms). During sliding rapid events occur at the wall–wall interface, and this rather than the CH_4 islands is likely to be the reason for the relatively high friction coefficient.

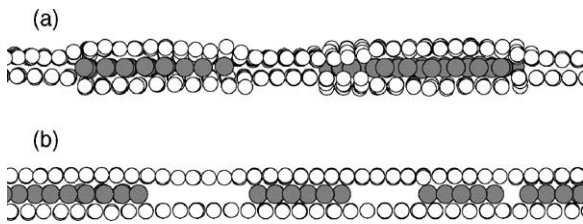


Fig. 24. (a) Snapshot picture of the lubricant system shown in Fig. 10; (b) snapshot picture of the lubricant system shown in Fig. 26. Vertical slices (xz -plane, $-10 \text{ \AA} < y < 10 \text{ \AA}$). Both calculations use the same model parameters, except that the elastic modulus is a factor 10 higher in case (b). In case (a) the combination of the external pressure and the wall–wall adhesion interaction is able to deform the solids so that complete wall–wall contact occurs between the CH_4 islands. In case (b) the elastic modulus is so high that only a very small “buckling” of the solid walls into the regions between the CH_4 islands occurs.

The elastic deformation of the solid walls around the CH_4 islands corresponds to a line energy. The system tries to minimize the (free energy) by reducing the line energy. This occurs, e.g. when two islands merge into a single island. In Fig. 25 we show a sequence of such snapshots which illustrates the merging of two CH_4 islands.

Let us now contrast the results above with results obtained for a system characterized by exactly the same parameters as used above, except that the elastic modulus now is 10 times higher, similar to that of gold. Fig. 26 shows a snapshot picture of the system which should be compared to Fig. 10, as obtained with a 10 times lower elastic modulus. In the present case the CH_4 molecules form a square lattice (or, equivalently, a $c(2 \times 2)$ structure relative to the block surface atoms) which is strongly pinned to the bottom surface of the block. During sliding there is no change in the structure of the CH_4 islands, and the islands follow the motion of the block. Because of the relatively high elastic modulus and strong pinning of the lubricant film to the block, there is practically no elastic instability happening in the present system and the sliding friction is extremely low, only $\mu_k \approx 1.7 \times 10^{-3}$ (at 10 m/s sliding velocity). The drastic difference

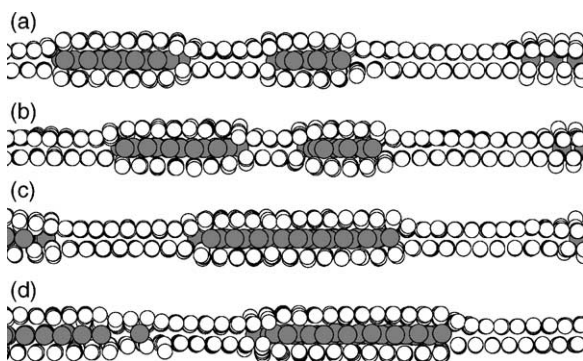


Fig. 25. A sequence of snapshot pictures during sliding ($v_s = 10 \text{ m/s}$), illustrating the merging of two CH_4 islands. Each picture shows a vertical slice (xz -plane, $-10 \text{ \AA} < y < 10 \text{ \AA}$). The snapshots are separated by equal time periods.

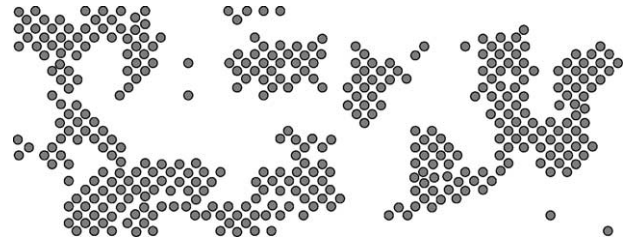


Fig. 26. Snapshot picture of a part of the contact area showing the lubrication film consisting of CH_4 molecules confined between two flat solid walls of gold, with the block and substrate atoms removed. Note that the CH_4 molecules (locally) form a commensurate (with respect to the block) square structure, which is pinned to the bottom surface of the block. This square structure remains during sliding. The CH_4 islands do not change their shapes during sliding, and different islands move with the same velocity. With $E = 7.7 \times 10^{10} \text{ Pa}$, $T = 10 \text{ K}$, $k_s = 30 \text{ N/m}$, $v_s = 10 \text{ m/s}$ and $P = 10^8 \text{ Pa}$.

between the systems in Figs. 10 and 26 is related to the difference in the elastic modulus of the solid walls which implies a much smaller relaxation of the solid walls into the regions between the CH_4 islands. This is illustrated in Fig. 24b. In Fig. 24a, the strong bending of the solids into the regions between the CH_4 islands will generate a strong line force which tends to squeeze together molecules in the CH_4 islands as much as possible; this is the reason for the close packed hexagonal CH_4 structure in this case. On the other hand, the boundary line force is negligible in the case shown in Fig. 24b and the CH_4 molecules take the square structure shown in Fig. 26 which maximizes the binding energy to the solid walls.

The boundary line forces, which are the origin of the merging of islands (see Fig. 25), and the compactification of islands (compare Fig. 10 with Fig. 26), also have other important manifestations, recently observed in Surface Forces Apparatus (SFA) measurements [40]. Thus, in one set of experiments, 2D islands of trapped lubricant fluid were observed after the squeeze-out of most of the lubricant. The islands slowly drifted towards the periphery of the contact area where they finally got squeezed out. The drift motion of the islands results from the Hertzian-like pressure distribution in the contact area. The line force acting on the island has a contribution (see [41]) proportional to the perpendicular Hertzian pressure $P(r)$, and since $P(r)$ is higher on the inner side (towards the center of the contact area) of the island, there will be a net force acting on the island in the direction towards the periphery of the contact area, resulting in a slow drift of the island towards the periphery of the contact area. SFA measurements have also shown that in some cases the line tension is so high that it compresses the monolayer islands into thicker islands, two or more monolayers thick (this process reduces the free energy of the system). The magnitude of the line tension is also important for the smoothness of the boundary line during squeeze-out.

Let us finally compare the results obtained above with results obtained for a system characterized by exactly the same parameters as used above (with $E = 7.7 \times 10^9 \text{ Pa}$,

$T = 10$ K, $k_s = 30$ N/m, $v_s = 10$ m/s and $P = 10^8$ Pa), except that the wall–wall interaction is equal to zero. In this case the CH₄ molecules form a square lattice (or a $c(2 \times 2)$ structure relative to the block surface atoms), which is strongly pinned to the bottom surface of the block, just as for the system shown in Fig. 26 (which is based on the same model but with 10 times higher elastic modulus of the solids and including wall–wall interaction). During sliding there is no change in the structure of the CH₄ islands, and the islands follow the motion of the block. Now, because of the absence of the wall–wall adhesion interaction, and because of the strong pinning of the lubricant film to the block, only very weak elastic instabilities occur in the present system, and the sliding friction is very small, only $\mu_k \approx 3.8 \times 10^{-3}$ (at 10 m/s sliding velocity). The drastic difference between the present system and that presented in Fig. 10 is related to the zero wall–wall adhesion interaction which (at moderate external pressure) gives a much smaller relaxation of the solid walls into the regions between the CH₄ islands. Thus, the side view of the present system is very similar to that shown in Fig. 24b. The very small bending of the solids into the regions between the CH₄ islands (but greater than in Fig. 24b), generates a weak line force which is not enough to squeeze the CH₄ islands into the high density hexagonal structure. Furthermore, many small islands (similar to those shown in Fig. 26) remain during sliding (i.e. no merging of islands). The structure of the islands (the CH₄ molecules form a square lattice structure (or $c(2 \times 2)$ structure relative to the block surface atoms)) is the same as in Fig. 26 since the line force is not strong enough to compress the islands (which would result in the CH₄ molecules forming the close packed hexagonal CH₄ structure shown in Fig. 10).

References

- [1] B.N.J. Persson, Sliding Friction: Physical Principles and Applications, 2nd ed., Springer, Heidelberg, 2000.
- [2] B.N.J. Persson, Surf. Sci. Rep. 33 (1999) 83.
- [3] B.N.J. Persson, P. Ballone, J. Chem. Phys. 112 (2000) 9524.
- [4] B.N.J. Persson, J. Chem. Phys. 113 (2000) 5477.
- [5] B.N.J. Persson, V.N. Samoilov, S. Zilberman, A. Nitzan, J. Chem. Phys. 117 (2002) 3897.
- [6] L. Bureau, T. Baumberger, C. Caroli, Eur. Phys. J. E 8 (2002) 331.
- [7] B.N.J. Persson, Eur. Phys. J., E 8 (2002) 385.
- [8] B.N.J. Persson, Phys. Rev. B 51 (1995) 13568.
- [9] J. Kurkijärvi, Phys. Rev. B 6 (1972) 832.
- [10] Y. Sang, M. Dube, M. Grant, Phys. Rev. Lett. 87 (2001) 174301.
- [11] O.K. Dudko, A.E. Filippov, J. Klafter, M. Urbakh, Chem. Phys. Lett. 352 (2002) 499.
- [12] E. Gnecco, R. Bennewitz, T. Gyalog, Ch. Loppacher, M. Bammerlin, E. Meyer, H.-J. Günterodt, Phys. Rev. Lett. 84 (2000) 1172; R. Bennewitz, E. Gnecco, T. Gyalog, E. Meyer, Tribol. Lett. 10 (2001) 51.
- [13] H. Matsukawa, H. Fukuyama, Phys. Rev. B 49 (1994) 17286.
- [14] B.N.J. Persson, J. Chem. Phys. 103 (1995) 3849.
- [15] P.A. Thomson, M.O. Robbins, Phys. Rev. A 41 (1990) 6830.
- [16] E.A. Jagla, Phys. Rev. Lett. 88 (2002) 245504.
- [17] V.L. Popov, Solid State Commun. 115 (2000) 369; V.L. Popov, B.N.J. Persson, MRS 651 (2000) T7.10.
- [18] O.M. Braun, M. Peyrard, Phys. Rev. E 63 (2001) 046110.
- [19] O.M. Braun, J. Röder, Phys. Rev. Lett. 88 (2002) 096102.
- [20] G. Blatter, M.V. Feigelman, V.B. Geshkenbein, A.I. Larkin, V.M. Vinokur, Rev. Mod. Phys. 66 (1994) 1125; G. Grüner, Rev. Mod. Phys. 60 (1988) 1129.
- [21] P. Chauve, T. Giamarchi, P. Le Doussal, Europhys. Lett. 44 (1998) 110.
- [22] O. Narayan, D.S. Fisher, Phys. Rev. B 46 (1992) 11520.
- [23] T. Nattermann, S. Stepanow, L.-H. Tang, H. Leschhorn, J. Phys. II 2 (1992) 1483.
- [24] B.N.J. Persson, V.L. Popov, Solid State Commun. 114 (2000) 261; B.N.J. Persson, J. Chem. Phys. 113 (2000) 5477; B.N.J. Persson, A.I. Volokitin, Surf. Sci. 457 (2000) 345; J. Crassous, L. Bocquet, S. Ciliberto, C. Laroche, Europhys. Lett. 47 (1999) 526.
- [25] P.A. Thompson, M.O. Robbins, Science 250 (1990) 792; P.A. Thompson, M.O. Robbins, Science 253 (1991) 916.
- [26] L. Bocquet, E. Charlaix, S. Ciliberto, J. Crassous, Nature 396 (1998) 735.
- [27] E. Riedo, F. Levy, H. Brune, Phys. Rev. Lett. 88 (2002) 185505.
- [28] J.H. Dietrich, B.D. Kilgore, Pure Appl. Geophys. 143 (1994) 283.
- [29] B.N.J. Persson, Phys. Rev. B 61 (2000) 5949.
- [30] T. Baumberger, C. Caroli, B. Perrin, O. Ronsin, Phys. Rev. E 51 (1995) 4005.
- [31] J.M. Carlson, A.A. Batista, Phys. Rev. E 53 (1996) 4153.
- [32] B.N.J. Persson, Phys. Rev. B 55 (1997) 8004.
- [33] G. He, M.H. Müser, M.O. Robbins, Science 284 (1999) 1650.
- [34] B.N.J. Persson, Phys. Rev. Lett. 87 (2001) 116101.
- [35] B.N.J. Persson, J. Chem. Phys. 115 (2001) 3840; B.N.J. Persson, F. Bucher, B. Chiaia, Phys. Rev. B 65 (2002) 184106.
- [36] M. Klüppel, G. Heinrich, Rubber Chem. Technol. 73 (2000) 578.
- [37] B.N.J. Persson, J. Chem. Phys. 115 (2001) 3840.
- [38] K.A. Grosch, Proc. R. Soc., Ser. A 274 (1963) 21.
- [39] N. Maeda, N. Chen, M. Tirrell, J. Israelachvili, Science 297 (2002) 379.
- [40] F. Mugele, M. Salmeron, Phys. Rev. Lett. 84 (2000) 5796; F. Mugele, private communication.
- [41] B.N.J. Persson, E. Tosatti, Phys. Rev. B 50 (1994) 5590; S. Zilberman, B.N.J. Persson, A. Nitzan, J. Chem. Phys. 115 (2001) 11268.